# IN-SITU EVAPORATION OF WATER WITHIN ROCK PILES – A MODELING AND LABORATORY STUDY

*Edward M. Trujillo and Paul S. Evans[1], University of Utah, Salt Lake City, UT, U.S.A.*

## Abstract

Acid rock drainage (ARD) is an environmental problem commonly faced by the mining industry. ARD occurs when sulfide-bearing rock, usually in the form of a large rock pile on the side of a mountain, is exposed to air and water and oxidizes to form sulfuric acid which can leach hazardous metal ions from various minerals. Laboratory tests are typically conducted using short columns packed with a crushed mining rock sample to determine a rock sample's potential to produce acid. The room temperature procedures that are typically involved in these tests are inherently non-isothermal because they involve a drying phase in which water evaporation occurs. We are investigating the processes that govern evaporation within a rock pile and the important parameters that describe these processes. A two-dimensional axially-symmetric model of the drying phase of the testing procedure has been developed by our research group. The model was developed using Darcy's law, heat transfer in porous media, and mass balance equations and was verified with an analytical solution under simplifying assumptions. The model was calibrated with experimental data from our laboratory for certain rock types. Hypothetical studies of the effects of heterogeneities in the form of inclined layers were also conducted.

## Introduction

ARD (acid rock drainage) is a very complex process occurring in nature as well as in mining operations. It occurs when sulfide-bearing rock, usually in the form of a large rock pile on the side of a mountain or in a tailings impoundment, is exposed to air and water and oxidizes to form sulfuric acid which can leach hazardous metal ions from various minerals. The processes include biological as well as geochemical and physical mechanisms but the main ingredients are air (oxygen), water and a sulfide mineral. In most cases, air flow is the limiting factor, primarily in tailings. However, due to the heterogeneity of rock piles, convective air currents can develop deep within the pile due to temperature gradients caused by exothermic oxidation reactions and these air currents can evaporate moisture within the pile and then condense it in other, cooler, locations.

Typically, the internal structure of the pile is not known and calibration of mathematical models describing the rock pile over time is limited to several field measurements taken from a few well bores throughout the pile at various time periods. Mathematical models that have been used in the past range from very simple homogeneous diffusion models to complex transport models with heterogeneous zones and containing several geochemical reactions. One aspect that has not been studied sufficiently is the process of drying and redistribution of water within the pile for arid and semi-arid regions. Many piles contain highly permeable zones, typically at inclined angles, that facilitate an up flow of air caused by temperature gradients within the pile, and thus allow the transport of gases, such as oxygen, water vapor, and carbon dioxide, to be distributed unevenly throughout the

[1] Now with Frontline BioEnergy, LLC

pile. In addition, entering dry air can evaporate some of the water contained in the pore structure and then condense that water in other parts of the pile that are cooler or have different humidity levels. Since ARD is dependent to a large degree on water saturation, it is important to understand the redistribution of water and water vapor over time and space. The objective of this study was to understand the equations and mechanisms involved in evaporation of water within rock piles in the laboratory in order to develop better models for field-scale studies.

Laboratory tests are conducted using columns packed with a crushed mining rock sample to determine a rock sample's potential to produce acid [ASTM, 2000]. The procedure typically involves a weekly cycle that contains a three-day drying period, a three-day moisture period and a one-day leaching period. The room temperature procedures that are typically involved in these tests can be non-isothermal if they involve a convective drying phase in which water evaporation occurs. Perhaps the most applicable study on evaporation from surfaces is the one done by Wilson *et al.* (1997). They were able to illustrate the effect of capillary pressure on the total drying rate using a soil water characteristic curve. They, however, did not actually model evaporation. The evaporative fluxes were simply compared to the evaporative flux from a sample in which there was no capillary pressure. Viollaz and Suarez (1985) give a short review of mass transfer correlations used to predict evaporative fluxes under various conditions. They then use numerical algorithms to find solutions to the problem of drying shrinking particles. Silva *et al.* (2000) studied porous media with very small pores (<5 nm.) in which Darcy's law was deemed invalid. They reported a method of estimating flow rates through the use of an effective diffusivity which was a function of many parameters such as porosity, tortuosity and pore size. Because waste rock piles have much larger pores (>>5 nm.) it is not reasonable to use this approach.

Stacey and Udell (1997) studied evaporation in porous media. They developed an analytical solution for the speed of an evaporation wave ($V_e$) traveling through a partially saturated porous medium by transforming the one-dimensional mass balance into wave coordinates. Their isothermal solution (given below) assumes phase equilibrium and no migration of water due to capillary pressure gradients.

$$V_e = \frac{u_d \rho_{id}}{\phi\left(S_{gd}\rho_{id} + S_{ld}\rho_{ld}\right)} \qquad [1]$$

In Equation 1 the subscript *d* represents the downstream condition. *u* is the superficial velocity of the gas phase. $\rho_i$ is the mass concentration of component i (the component being evaporated) and $\rho_l$ is the liquid density. Equation 1 can be used to give a good estimate of the time it will take to completely dry an isothermal unsaturated sample. However, drying is rarely an isothermal process. Stacey and Udell also give analytical solutions for the temperature drop due to evaporation ($\Delta T$) and the propagation speed ($V_T$) of the thermal wave. Their solutions were compared to numerical models and experimental data with reasonable agreement. They conclude that an isothermal treatment will almost always over predict evaporation rates in porous media.

## Experimental Apparatus and Procedure

A typical humidity cell is constructed of Lexan or similar plastic material and is four inches in diameter and eight inches tall. The cell has a removable lid, which allows the rock sample to be placed onto a felt pad that is supported by a perforated plastic disk. Air flows from the bottom

upwards through a side port below the perforated disk while the aqueous leachate flows out the bottom. Procedures typically follow that in ASTM standard methods [ASTM, 2000] however, in this project, temperature probes were added to measure transient temperatures within the humidity cell sample.

Four Omega brand PR-17 RTD probes were fitted to each cell to in order to measure temperature at different locations in the humidity cell during testing. According to the literature the probes give readings with an accuracy of ±0.3º C for a temperature range of -25º C to 85º C (Pace Scientific, 2005). The four RTD probes were inserted into the humidity cells, at heights of 0.8, 3.3, 5.7 and 8.0 cm from the top of the polypropylene felt. Cell F11 contained waste rock from a mining site in the western United States, while crushed marble was used for the control cell. An Opto22 control system was used to continuously record the temperatures measured by the RTD probes at predetermined intervals. Figure 1 shows the control cell packed with crushed marble. The picture shows the location of the temperature probes. Note that the top probe is located at the top surface of the rock material. Figure 2 shows a similar cell packed with an acid-producing rock sample (F11) from a mining site. Note that, in this cell, the top probe is about one inch above the rock surface, since the particle size and bulk density are different than that of the crushed marble. Only data taken with the bottom three probes were used for calibration of the model.

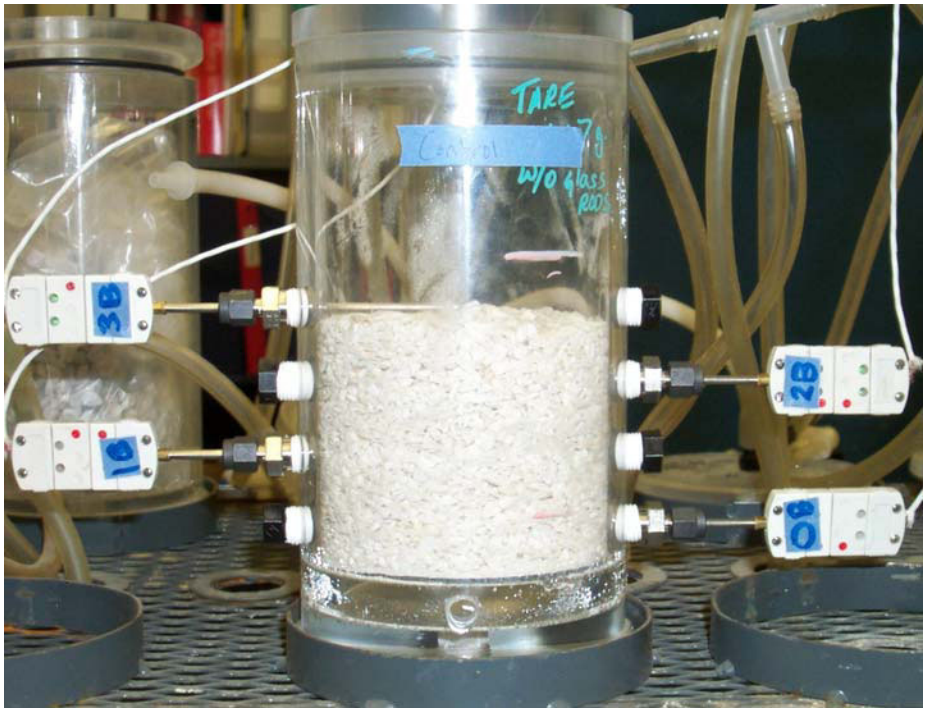


**Figure 1 A humidity cell containing crushed marble, used as the control cell. Also shown are the locations of the RTD probes, which are approximately 1 inch apart.**

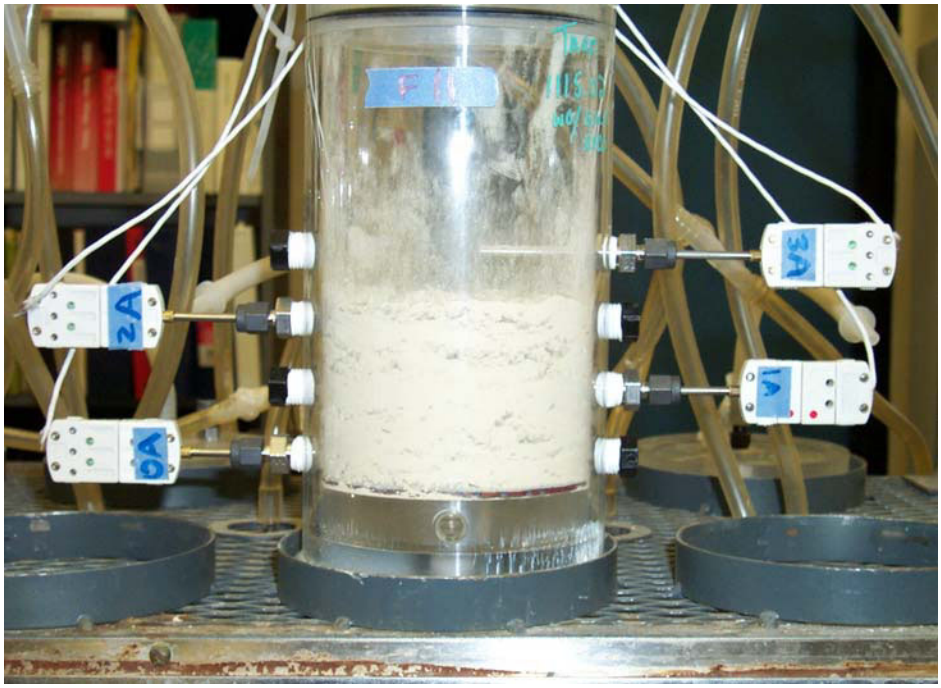


**Figure 2 A humidity cell containing sample F11, an acid-producing sample. Also shown are the locations of the RTD probes, which are approximately 1 inch apart.**

## Modeling

Comsol Multiphysics™ (Comsol, 2007), a finite element based computer program, was used to create the humidity cell models. As multi-physics software, Comsol has many modules which can be used to assist in modeling physical phenomena. Ambient conditions were assumed to be standard temperature and pressure. The thermal conductivities of air and water as functions of temperature were given by the expressions used by Eldredge (2005). Other thermal conductivities were assumed to change insignificantly over the temperature range of interest. The enthalpy of vaporization of water was also assumed to change very little over the temperature interval and was therefore treated as a constant. The Clausius Clapyeron equation was used to predict the saturation vapor pressure of water as a function of temperature. Water's normal boiling point was used for the reference condition. Additionally, the solid phase was assumed to be immobile. Several models were developed for the project:

- A 1D Isothermal model
- A 1D Adiabatic model
- A 1D Non-adiabatic model
- A 2D Non-adiabatic Homogeneous model
- A 2D Non-adiabatic Heterogeneous model .

For this paper we will only discuss the 1D isothermal model, the 1D non-adiabatic model and the 2D non-adiabatic heterogeneous model. P.S. Evans describes all these models in more detail [Evans, 2007]

**1D Isothermal Evaporative Model**

The isothermal case was run using two mass balances, one for liquid and one for vapor phase water. Concentration ($c$) of each species is determined by solving the continuity equation at each element.

$$\frac{\partial c}{\partial t} + \nabla \cdot \left( \vec{u} c - D \nabla c \right) = R \qquad [2]$$

Evaporation was accounted for using the reaction term ($R$). The evaporation rate was determined from the flux of water vapor from the liquid surface which was then multiplied by the specific surface area ($Ai$) of the medium. Although the liquid surface area will change with saturation, it was assumed have a constant value equal to that of uniform cubic face center packed spheres. A conceptual diagram of the 1D model is given in Figure 3 below.

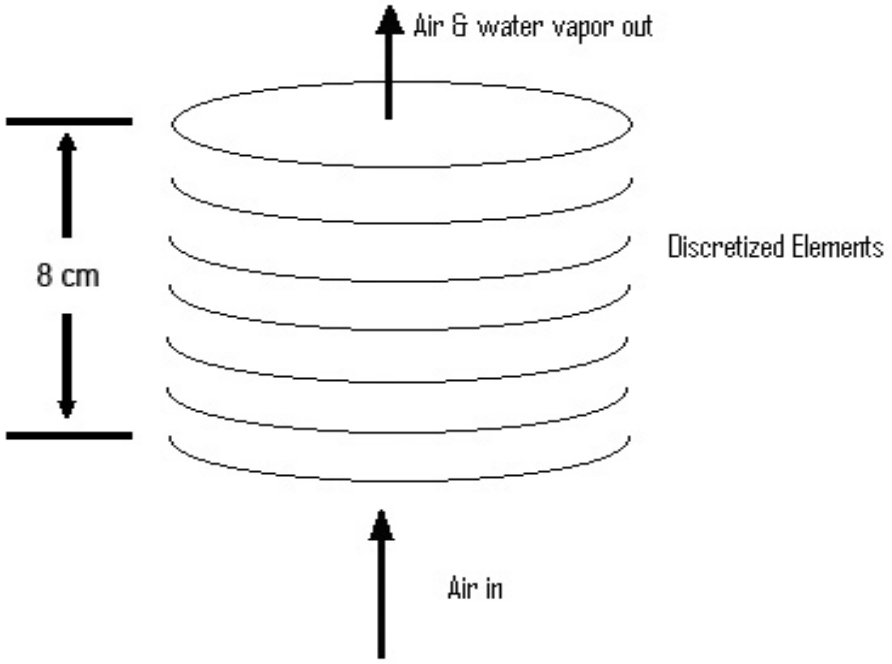


**Figure 3 Conceptual diagram of the 1D evaporation model. Note, not all mesh elements have been shown.**

The liquid phase velocity was assumed to be zero, while the vapor phase velocity was set to the superficial velocity of the entering air. This neglects a small increase in vapor phase velocity due to evaporation. This assumption was made because the equilibrium vapor pressure of water at the temperatures of interest is much less than one atmosphere. The liquid phase diffusivity was set to a very small number, but not zero. This gave stability to the numerical solution, while simulating the

wicking that arises due to capillary action.

A zero flux boundary condition was given to the liquid mass balance at both boundaries. The concentration of the water vapor was set to zero at the inlet, and a convective flux boundary condition (no diffusive flux) was applied at the outlet. Table 1 provides a summary of the parameters used for the 1D isothermal evaporative model, which are applicable to Cell F11.

**Table 1 Parameters used in the 1D isothermal evaporative model for Cell F11**

| Parameter | Symbol | Value | Units | Reference |
|---|---|---|---|---|
| Porosity | $\varphi$ | 0.36 | – | Eldredge, 2005 |
| Initial saturation | $S_0$ | 0.44 | – | Klinker, 2006 |
| Initial & ambient temperature | $T_0$ | 298 | Kelvin | Klinker, 2006 |
| Air flow rate | $q_{air}$ | 1 | Lpm | Klinker, 2006 |
| Inner diameter of humidity cell | $D$ | 10 | cm | Eldredge, 2005 |
| Height of sample in cell | $h$ | 8 | cm | Klinker, 2006 |
| Mass transfer Peclet Number | $Pe_m$ | 0.06 | – | calculated |
| Lumped mass transfer coefficient | $kA$ | 100,000 | $s^{-1}$ | Bird, 2002 |

Figure 4 gives the results of the one dimensional isothermal model for the set of parameters given in Table 1. The lumped mass transfer coefficient ($kA$) is the product of the mass transfer coefficient and the specific surface area used to calculate total evaporative flux per unit volume using equation 2.19. Figure 4 gives the water saturation profile within the cell at $5x10^4$ seconds and shows a relatively sharp front with the rock sample essentially drying out completely after the front moves through. For easy comparison with the analytical solution (Equation 1) a vertical black line has been included to indicate the position of the evaporation front at $5x10^4$ seconds, as predicted by the analytical expression. It was found that the evaporation rate is insensitive to the mass transfer coefficient and the specific surface area above a threshold surface value. This indicates that, because the pore spaces are so small, the water vapor is able to come to equilibrium almost instantly. This is to be expected with such a small Peclet Number (0.06). This may not be the case for much larger rock particles or in situations with a much higher convective velocity.

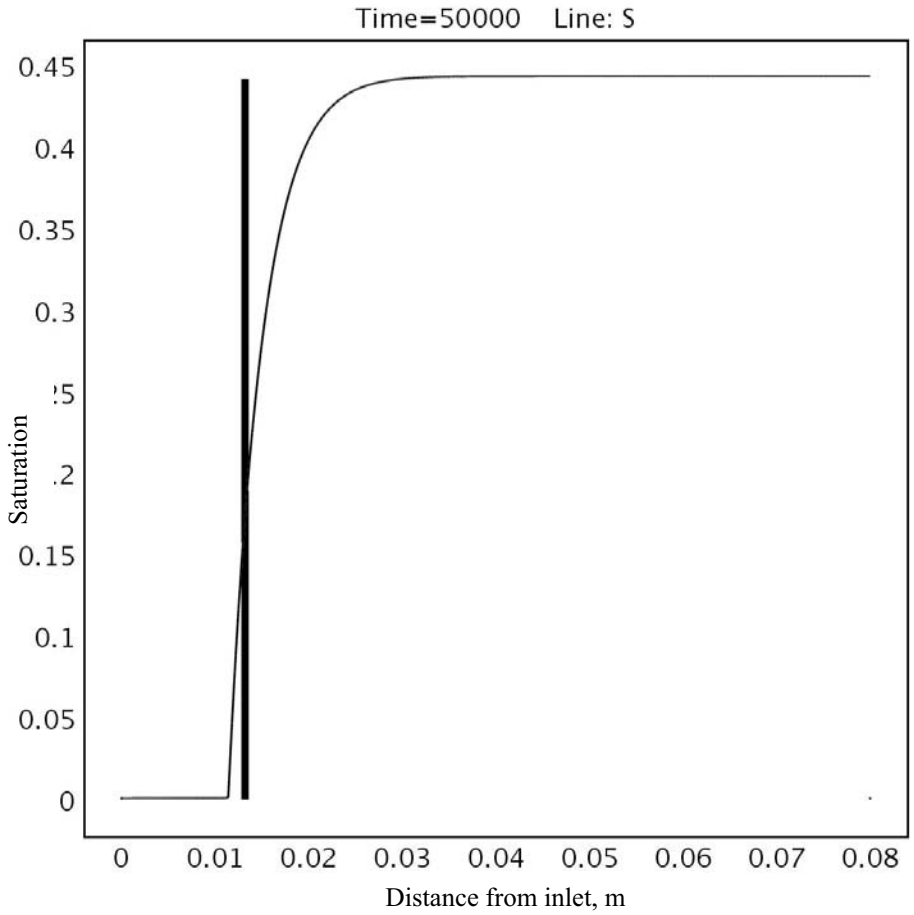


**Figure 4 Saturation (Y axis) as a function of distance from inlet in meters (X axis) after 50,000 seconds as predicted by the 1D isothermal model. The vertical line indicates the position of the evaporation front according to the analytical solution (Equation 1).**

**1D Nonadiabatic Evaporative Model**

In order to have a numerical model to compare to experimental results, a non-adiabatic model was developed to account for heat transfer with the surroundings. Due to the one-dimensional nature of this model some simplifications had to be made with regard to heat transfer in the radial direction. Incropera and DeWitt (2002) give the steady state solution to the radial heat transfer rate ($q_r$) as the following.

$$q_r = \frac{T - T_\infty}{\frac{\ln\left(r_i / r_r\right)}{2\pi L \lambda_r} + \frac{\ln\left(r_o / r_i\right)}{2\pi L \lambda_w} + \frac{1}{2\pi L r_o h}} \qquad [3]$$

In Equation 3, the subscripts *r* and *w* refer to properties of the rock and the humidity cell wall, respectively. $r_i$ and $r_o$ are the inner and outer radii of the cylinder and *h* is a convective heat transfer

coefficient. The temperature of the surface of the cell was assumed to have a constant value equal to the ambient temperature ($T_\infty$). This is the same as saying that the last resistance term in the denominator is much less than either of the other two terms. Additionally, the first resistance term vanishes under the assumption that the rock has no radial temperature gradient (it is a 1D problem). In order to be included in the volumetric heat generation term, $q_r$ must be divided by the total volume of the porous medium. Thus, as might be expected, the volumetric heat generation due to radial conduction ($Q_r$) is independent of the length of the cell ($L$).

$$Q_r = \frac{2\lambda_w (T - T_\infty)}{r_i^2 \ln\left(r_o / r_i\right)} \qquad [4]$$

The boundary conditions used were all the same as in the previous model, but with one exception. The temperature was not held constant at the inlet. Instead, a heat flux boundary condition was applied. The heat flux was determined from the enthalpy and flow rate of the incoming air. To model Cell F11, the non-adiabatic model used the same parameters as the adiabatic model, with the addition of the thermal conductivities of the humidity cell wall and the insulation used by Klinker (2006). These are given in Table 2. The control cell was also simulated using the 1D non-adiabatic model. The differences in the thermal properties of the control cell as compared with Cell F11 were insignificant. Therefore, when adjusting the model to represent the control cell, the only parameters that needed to be changed were the porosity and the initial saturation, which were 45% and 16%, respectively (Eldredge, 2005).

**Table 2 – Parameters used in the 1D nonadiabatic evaporative model for Cell F11 and the Control Cell**

| Parameter | Symbol | Value | Units | Reference |
|---|---|---|---|---|
| Thermal conductivity of solids | $k_s$ | 2.5 | W m$^{-1}$ K$^{-1}$ | Eldredge, 2005 |
| Thermal conductivity of plexiglass | $k_p$ | 0.2 | W m$^{-1}$ K$^{-1}$ | Incropera & DeWitt, 2002 |
| Thermal conductivity of Insulation | $k_i$ | 0.08 | W m$^{-1}$ K$^{-1}$ | Incropera & DeWitt, 2002 |

Figures 5 and 6 show the results of the one dimensional non-adiabatic model. The experimental data from Klinker (2006) have also been shown for comparison. The following two figures display the results of the 1D nonadiabatic model for each humidity cell along with the respective experimental data from Week One. The experimental data exhibits small fluctuations in temperature which are seen on both sets of data (F11 and Control). This is likely due to changes in ambient temperature.

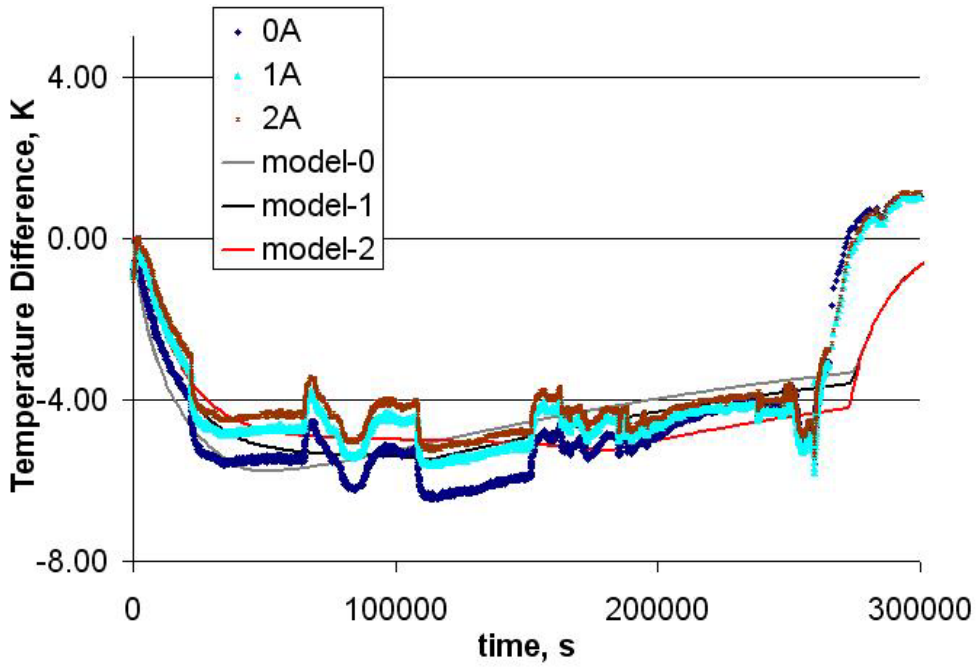


**Figure 5 Experimentally determined and model predicted temperatures in humidity cell F11, Week One. 0A, 1A and 2A are the bottom, middle and top RTD probes respectively. Model points 0, 1 and 2 are the temperatures predicted by the 1D non-adiabatic model at the corresponding distances from the inlet of the humidity cell. Initial saturation was set at 44%.**

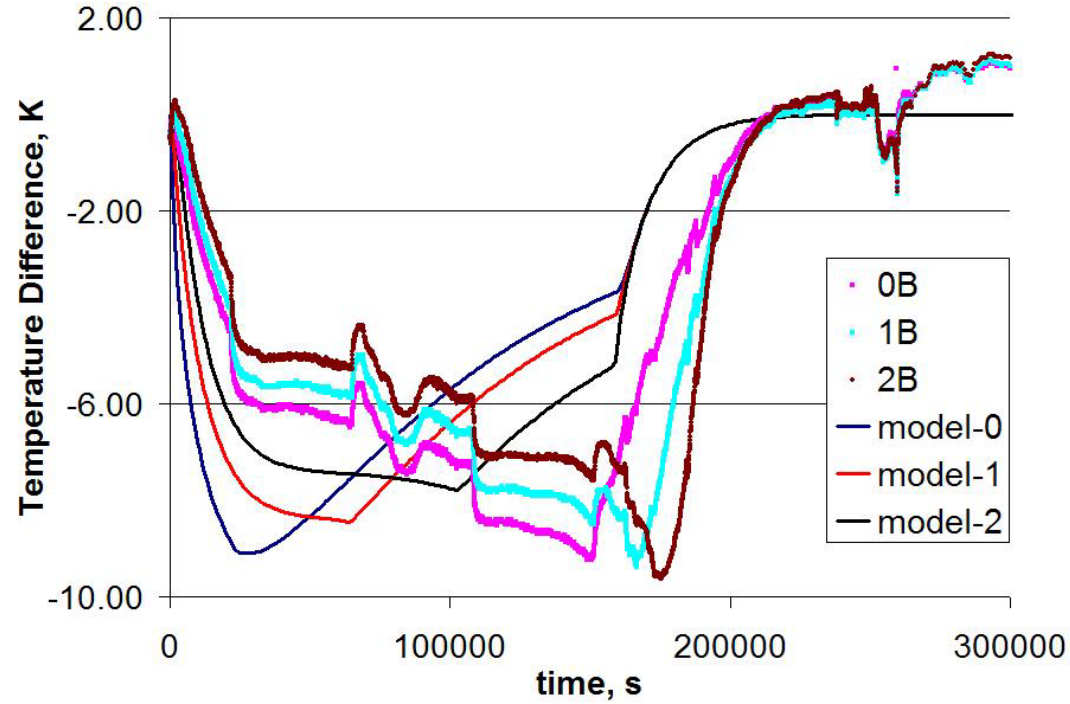


**Figure 6 Experimentally measured and model predicted temperatures in the control cell, Week One. 0A, 1A and 2A are the bottom, middle and top RTD probes respectively. Model points 0, 1 and 2 are the temperatures predicted by the 1D non-adiabatic model at the corresponding distances from the inlet of the humidity cell. Initial saturation was set at 16% in the model.**

It has been observed that the humidity cell does not always retain the same amount of water each week (Eldredge, 2005). There can also be settling from week to week. Because of this, it may be necessary to adjust the initial saturation and even sometimes the porosity, in order to match the experimental data. After making minor adjustments to the initial saturation, the non-adiabatic model was able to predict the temperature in the humidity cell with good agreement to the experimentally collected data. The best fit was obtained by raising the initial saturation of the Control Cell from 16% to 19%. The initial saturation of Cell F11 was lowered from 44% to 40%. It was not necessary to adjust the porosity for either of the humidity cells to obtain a good fit with the experimental data.

**2D Heterogeneous Evaporative Model**

A two-dimensional axis-symmetric model of the evaporation phase was also developed (see Figure 7). The mass balances used were the same as those already described for the 1D problem. The energy balance is essentially the same as well. The temperature of the wall of the humidity cell was held constant. A zero flux boundary condition was applied to both mass balance equations along the cell wall. All the parameters used in this model were the same as those of the 1D non-adiabatic model.

In the heterogeneous model an inclined layer was introduced to the domain in order to examine the effect of an irregular flow field (Figure 7). It should be noted that this layer, in cylindrical coordinates, is actually shaped like a hollow cone. Two heterogeneous scenarios were run. In the first one, the inclined layer was given a permeability four orders of magnitude higher than the surrounding rock. In the second, the permeabilities were switched such that the inclined layer had the lower permeability. For transient problems the following equation is solved.

$$\left[\beta(1-\phi)+\alpha\phi\right]\frac{\partial P}{\partial t}+\nabla\cdot\frac{k}{\mu}\nabla\left(P+\rho g z\right)=Q_s \qquad . \qquad [5]$$

The solid was assumed to be incompressible ($\beta = 0$)and air was given the compressibility of an ideal gas ($\alpha = 1/P$. The evaporation rate was used for the source term ($Q_s$). The parameters for the 2D heterogeneous evaporative model are the same as those for the 1D nonadiabatic model; also, this model requires additional parameters for Darcy's law which can be found in Table 3.

The boundary conditions used for this model were the same as those used for the homogeneous model. Additionally a constant velocity boundary condition was used at the inlet and a constant pressure boundary condition was used at the outlet for the momentum balance. A zero flux boundary condition was used on the cell wall.

**Table 3 – Darcy's Law parameters used in the 2D heterogeneous models**

| Parameter | Symbol | Value | Units | Reference |
|---|---|---|---|---|
| High permeability | $k$ | $1\text{x}10^{-5}$ | $m^2$ | Schwartz & Zhang, 2003 |
| Low permeability | $k$ | $1\text{x}10^{-9}$ | $m^2$ | Schwartz & Zhang, 2003 |
| Viscosity of Air | $\mu_a$ | $1.8\text{x}10^{-5}$ | Pa s | Incropera & DeWitt, 2002 |

With this geometry, it was observed at the four corners of the inclined layer that the energy balance predicted local temperature irregularities which did not appear to be physically realistic. This was likely due to a numerical effect of a single mesh element into which flow converges or diverges. No matter how fine the mesh, there would always be a single element in the vertex. This was remedied by "rounding the corners." After smoothing the mesh in this manner the hot and cold spots disappeared.

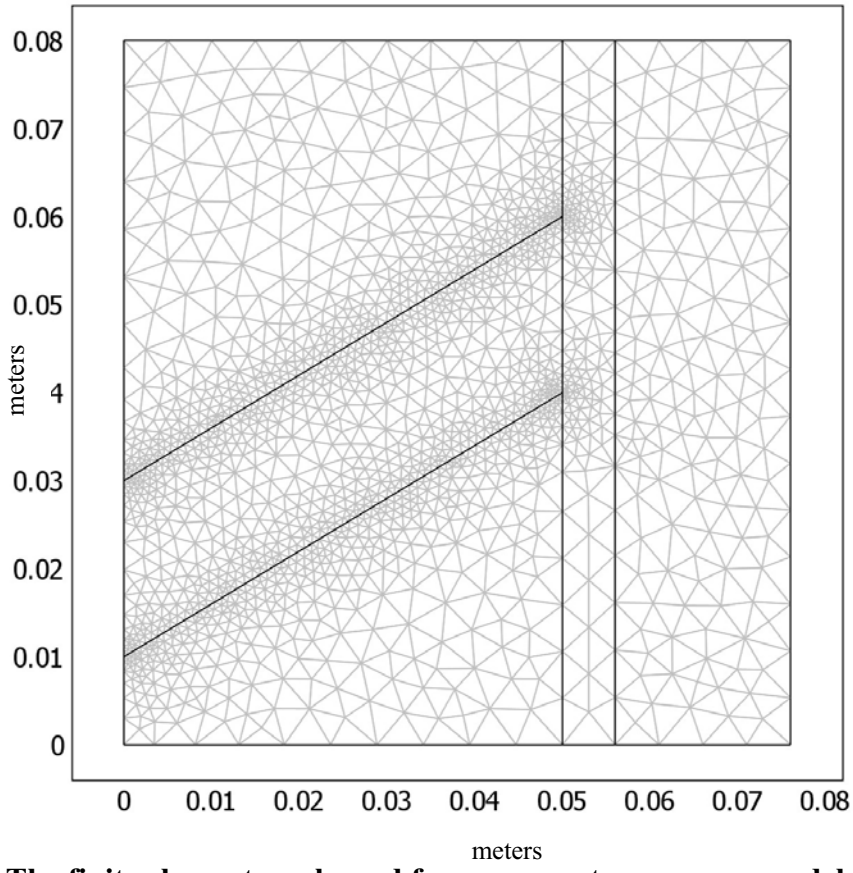


**Figure 7 The finite element mesh used for the 2D heterogeneous model. Note the high density of mesh elements at the transition between zones of different permeability. The scale is in meters.**

**High permeability layer**

Figure 8 shows a higher radial temperature gradient within the humidity cell than was exhibited by the homogeneous model (not shown). There is a difference in temperature of nearly two Kelvin from the center to the inner edge of the humidity cell. This is roughly double that of the homogeneous 2D evaporative model. This is due to the fact that the flow field is no longer uniform in the radial direction (see Figures 8 and 9). Figure 9 shows how the irregular flow field gives rise to an irregular evaporation front, which explains the higher radial temperature gradient.

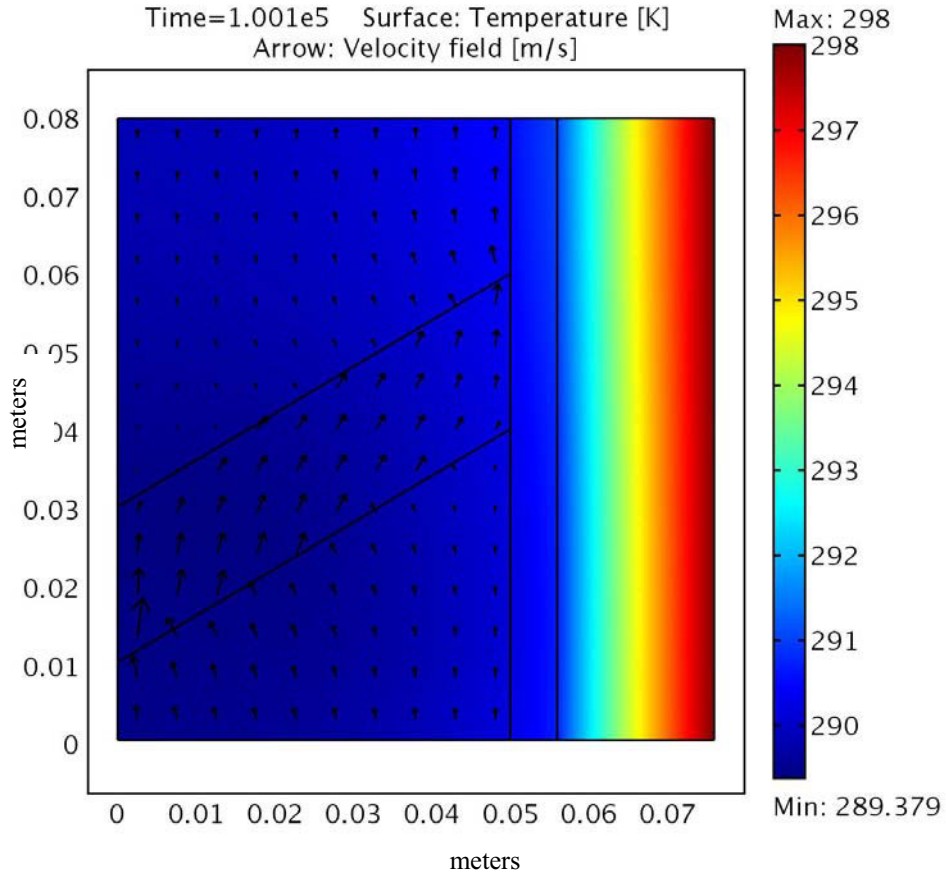


**Figure 8 Temperature (color scale) and flow field (arrows) in the 2D humidity cell model with a layer of high permeability material after $1x10^5$ s. Note that the air flow through the high permeability layer is nearly parallel to its orientation. Also note the modest radial temperature gradient in the medium. The x and y axes are given in meters.**

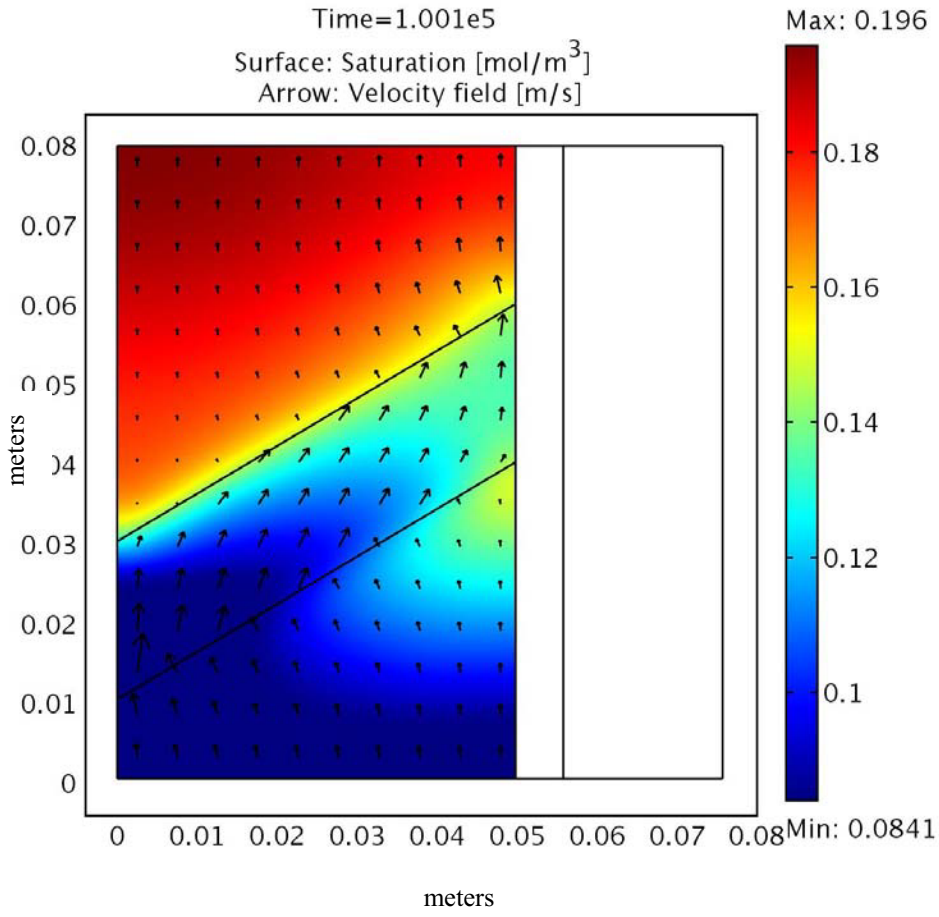


**Figure 9 Saturation (color scale) and flow field (arrows) in the humidity cell with a high permeability layer after $1x10^5$ s. Note the irregular evaporation front. The x and y axes are given in meters.**

**Low permeability layer**

The flow fields predicted by the model in the heterogeneous cases are what would be expected. The air moves through the low permeability layer in a direction perpendicular to the interface, while the air moves in a nearly parallel direction through the high permeability layer (Compare Figure 9 to 11). The radial temperature gradient within the humidity cell with the low permeability layer is roughly the same as that of the previous case. Figure 11 shows that the evaporation front is also irregular. However, this irregularity is not as pronounced as it was in the previous case (with the high permeability layer). The transient temperature profile in the low permeability layer 2D heterogeneous evaporative model appears to be roughly the same as with the high permeability layer.

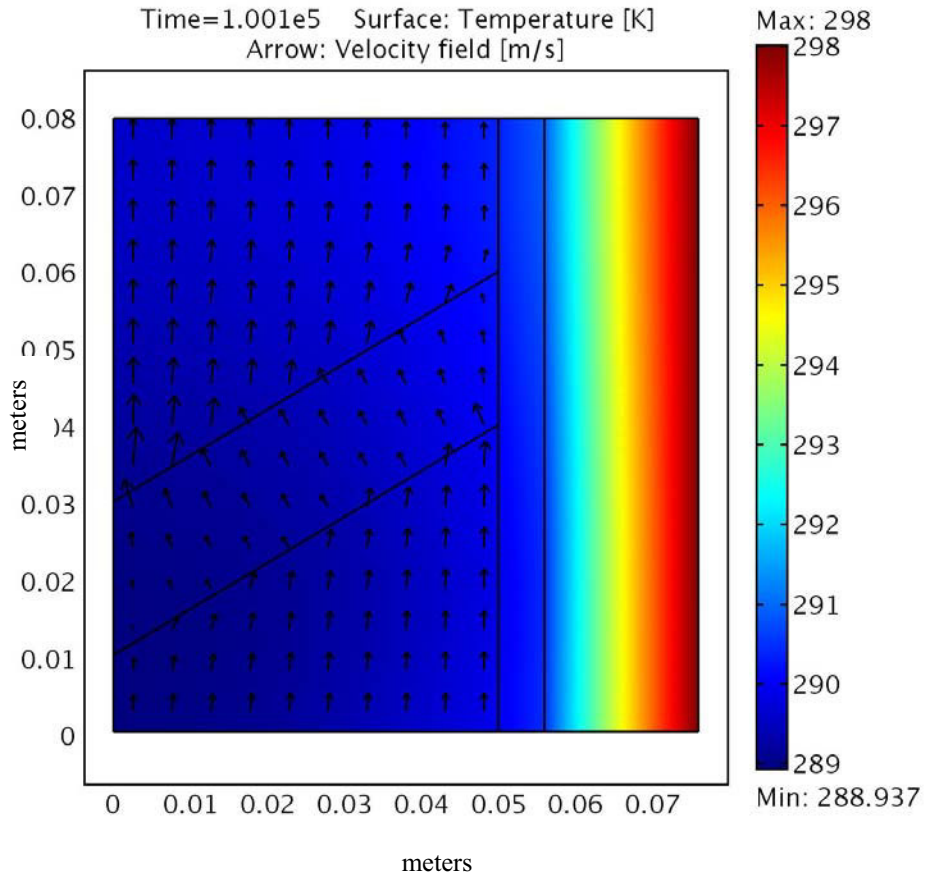


**Figure 10 Temperature (color scale) and flow field (arrows) in the humidity cell with a layer of low permeability material after $1x10^5$ s. Note that the air flow in the low permeability layer is roughly perpendicular to its orientation. Also note the radial temperature gradient. The x and y axes are both given in meters.**

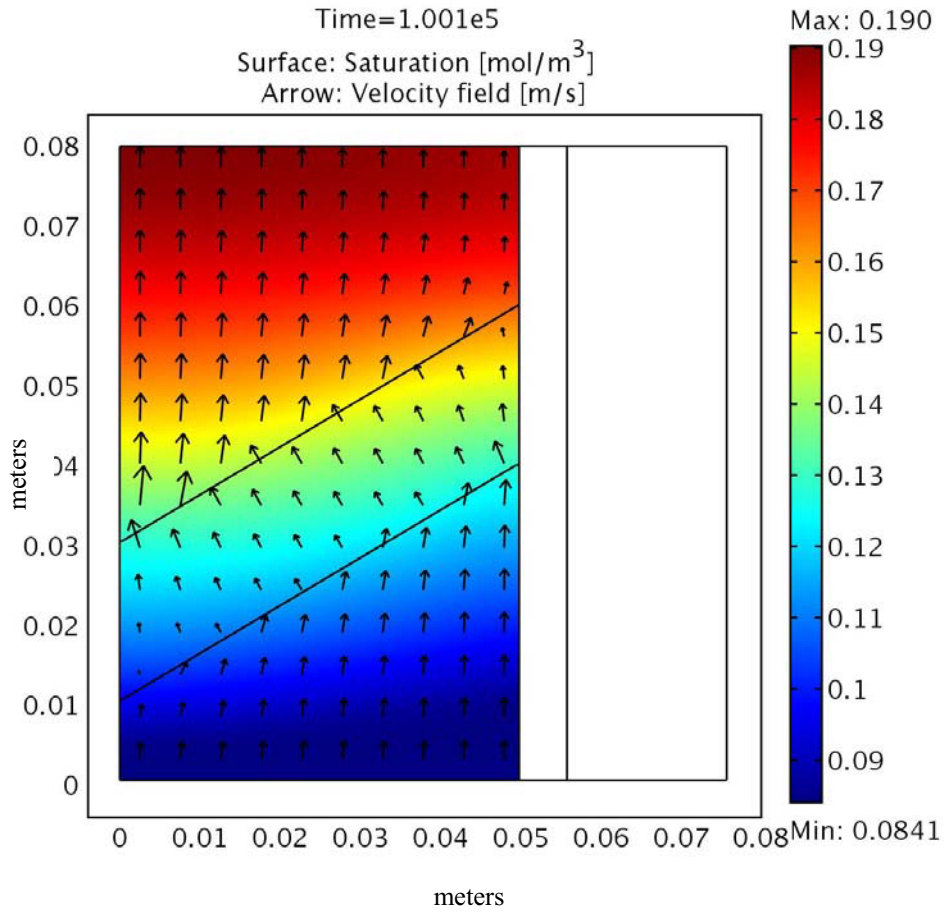


**Figure 11 Saturation (color scale) and flow field (arrows) in the humidity cell with a low permeability layer after 1x10$^5$ s. Note the irregular evaporation front. The x and y axes are given in meters.**

## CONCLUSIONS AND FUTURE WORK

The one dimensional isothermal model shows excellent agreement with the analytical solution. The one-dimensional non-adiabatic evaporative model is capable of matching the temperature changes observed experimentally in the humidity cell. The model is relatively insensitive to the thermal conductivity of the composite rock material. It has also been found that the evaporation rate is insensitive to the mass transfer coefficient and the specific surface area above a threshold surface area. This indicates that, because the pore spaces are so small, the water vapor is able to come to equilibrium almost instantly. Therefore, for the purposes of modeling evaporation in crushed rock, it is not important to determine the mass transfer coefficient or the surface area of the porous medium with a high degree of accuracy. Heterogeneities in the porous media, however, can distort the flow patterns and can influence the amount and rate of evaporation.

ARD occurs over time scales of tens and hundreds of years. In continuation of this work, we plan to develop a model that will simulate all three phases of the humidity cell and include several geochemical and biological reactions that are involved in ARD over these time periods. We intend to compare our weekly simulations with not only the drying phase of the experimental procedure, but the leaching phase as well, so that we can compare the predicted leachate water quality with experimental data for a number of ions in hopes of generating kinetic rate constants. Thus, we hope to accurately capture the important aspects of humidity cell weathering that will help explain the weathering experienced in the field on a much larger scale and help predict the effects on the environment and rock pile stability.

***Acknowledgement:***

We would like to thank Chevron Mining, Inc. and the US Bureau of Land Management (Salt Lake City office) for their financial support. We would also like to thank Wes Eldredge and Andrew Klinker for assistance with the modeling and conducting the experiments.

## REFERENCES

**ASTM,** "D 5744-96, Standard Test Method for Accelerated Weathering of Solid Materials Using a Modified Humidity Cell," in "Annual Book of ASTM Standards, 11.04". American Society for Testing and Materials, West Conschohocken, PA. (2000).

**Bird, R.B.; Stewart, W.E.; Lightfoot, E.N.,** "Transport Phenomena," 2nd ed. John Wiley and Sons, New York (2002).

**Comsol Group,** http://comsol.com/, (Apr. 2007).

**Eldredge, W.M.,** "Modeling Evaporation in Laboratory Rock Samples," M.S. Thesis, University of Utah: Chemical Engineering Dept., Salt Lake City, UT (2005).

**Evans, P.S.,** "Modeling the Effects of Evaporation on Acid Rock Drainage in Mine Rock Samples," M.S. Thesis, University of Utah: Chemical Engineering Dept., Salt Lake City, UT (2007).

**Incropera, F.P.; DeWitt, D.P.,** "Fundamentals of Heat and Mass Transfer," John Wiley and Sons, New York (2002).

**Klinker, A.D.,** "Flow Effects on Temperature Controlled Humidity Cells," B.S. Thesis, University of Utah: Chemical Engineering Dept., Salt Lake City, UT (2006).

**Pace Scientific,** Staff Homepage, Temperature Probes, http://www.pace-sci.com/temperature-xr5.htm ( July 8, 2005).

**Stacey, D.A., and Udell, K.S.,** "Propagation of the Thermal and Evaporation Waves Through a Water-Wet Porous Media During Through-Flow Air Drying," Proceedings, Heat Transfer and Fluids Engineering, ASME (1997).

**Schwartz, F.W.; Zhang, H.,** "Fundamentals of Groundwater," John Wiley and Sons, New York (2003).

**Silva, M.A.; Kerkhof, P.J.A.M.; Coumans, W.J.,** "Estimation of Effective Diffusivity in Drying of Heterogeneous Porous Media," *Ind. Eng. Chem. Res*., **39** (5) (2000).

**Viollaz, P.; Suarez, C.**, "Drying of Shrinking Bodies," *AIChE Journal,* **31** (9) (1985).

**Wilson, G.W.; Fredlund, D.G.; Barbour, S.L.,** "The Effect of Soil Suction on Evaporative Fluxes from Soil Surfaces." *Can. Geotech. J*., **34** pp. 145-155 (1997).